GLOBAL CARDIOLOGY SCIENCE & PRACTICE

A Qatar Foundation Academic Journal

OPEN ACCESS

Research article

Computational fluid dynamics applied to virtually deployed drug-eluting coronary bioresorbable scaffolds: Clinical translations derived from a proof-of-concept

Bill D. Gogas[1,6,†], Boyi Yang[2,6,†], Tiziano Passerini[2], Alessandro Veneziani[2,6], Marina Piccinelli[3,6], Gaetano Esposito[2,6], Emad Rasoul-Arzrumly[1,6], Mosaab Awad[1], Girum Mekonnen[1,6], Olivia Y. Hung[1,6], Beth Holloway[1,6], Michael McDaniel[1,6], Don Giddens[4,6], Spencer B. King III[1,5,6], Habib Samady[1,6,*]

[1]Andreas Gruentzig Cardiovascular Center, Department of Medicine, Division of Cardiology, Emory University School of Medicine, Atlanta, Georgia
[2]Department of Mathematics and Computer Science, Emory University, Atlanta, Georgia
[3]Department of Radiology and Imaging Sciences, Emory University, Atlanta, Georgia
[4]Wallace H. Coulter Department of Biomedical Engineering, Georgia Institute of Technology and Emory University, Atlanta, Georgia
[5]Saint Joseph's Heart and Vascular Institute, Atlanta, Georgia
[6]Emory GT Imaging Biomechanical Core Laboratory, Emory University School of Medicine, Atlanta, Georgia
[†]Both authors contributed equally to this manuscript
*Email: hsamady@emory.edu

ABSTRACT

Background: Three-dimensional design simulations of coronary metallic stents utilizing mathematical and computational algorithms have emerged as important tools for understanding biomechanical stent properties, predicting the interaction of the implanted platform with the adjacent tissue, and informing stent design enhancements. Herein, we demonstrate the hemodynamic implications following virtual implantation of bioresorbable scaffolds using finite element methods and advanced computational fluid dynamics (CFD) simulations to visualize the device-flow interaction immediately after implantation and following scaffold resorption over time.

Methods and Results: CFD simulations with time averaged wall shear stress (WSS) quantification following virtual bioresorbable scaffold deployment in idealized straight and curved geometries were performed. WSS was calculated at the inflow, endoluminal surface (top surface of the strut), and outflow of each strut surface post-procedure (stage I) and at a time point when 33% of scaffold resorption has occurred (stage II). The average WSS at stage I over the inflow and outflow surfaces was 3.2 and 3.1 dynes/cm² respectively and 87.5 dynes/cm² over endoluminal strut surface in the straight vessel. From stage I to stage II, WSS increased by 100% and 142% over the inflow and outflow surfaces, respectively, and decreased by 27% over the endoluminal strut surface. In a curved vessel, WSS change became more evident in the inner curvature with an increase of 63% over the inflow and 66% over the outflow strut surfaces. Similar analysis at the proximal and distal edges demonstrated a large increase of 486% at the lateral outflow surface of the proximal scaffold edge.

Conclusions: The implementation of CFD simulations over virtually deployed bioresorbable scaffolds demonstrates the transient nature of device/flow interactions as the bioresorption process progresses over time. Such hemodynamic device modeling is expected to guide future bioresorbable scaffold design.

Keywords: bioresorbable scaffolds, computational fluid dynamics, virtual modeling

http://dx.doi.org/10.5339/gcsp.2014.56

Submitted: 7 October 2014
Accepted: 11 December 2014

Cite this article as: Gogas BD, Yang B, Passerini T, Veneziani A, Piccinelli M, Esposito G Rasoul-Arzrumly E, Awad M, Mekonnen G, Hung OY, Holloway B, McDaniel M, Giddens DP, King III SB, Samady H. Computational fluid dynamics applied to virtually deployed drug-eluting coronary bioresorbable scaffolds: Clinical translations derived from a proof-of-concept, *Global Cardiology Science and Practice* 2014:56 http://dx.doi.org/10.5339/gcsp.2014.56

QSCIENCE.com

An Initiative of Qatar Foundation

INTRODUCTION

Despite tremendous innovations in platform design such as strut thickness reductions, use of novel antiproliferative agents, coatings with bioresorbable polymers or abluminal drug coatings,[1] the utilization of a permanent metallic prosthesis for the treatment of significant coronary artery disease remains a precipitating factor for sustained vascular inflammation, in-stent neoatherosclerosis and impaired vasomotor function.[2] Therefore, the concept of a drug-eluting bioresorbable scaffold with properties that allow short-term temporary scaffolding and long-term restoration of vascular physiology and anatomy when the device is fully resorbed is appealing. Several drug-eluting bioresorbable devices, such as the Absorb bioresorbable vascular scaffold (Abbott Vascular, SC, Calif.), the DESolve bioresorbable scaffold, (Elixir Medical, Sunnyvale, Calif.), and the Drug Eluting Absorbable Metal Scaffold (DREAMS) (Biotronik, Bülach, Switzerland) have been clinically tested in first-in-man studies utilizing multi modality imaging techniques showing encouraging clinical results up to 3-years. These endeavors have led the development of a novel field in interventional cardiology, that of vascular reparation therapy.[3]

Recent data suggest that variations in the local hemodynamic environment post stenting result in wall shear stress (WSS) regional alterations that can invoke a differential vascular healing response around the stent struts.[4] The vessel geometry after stenting is determined by several factors which influence vascular angulation and curvature including material properties of the implanted device, strut thickness and underlying plaque composition. By design, bioresorbable devices have thicker struts in order to retain the necessary scaffolding; meanwhile strut resorption associated with vascular healing over time balances the hemodynamic impairment observed during the post-implantation stage. Furthermore bioresorbable devices offer a more compliant platform that limits vascular straightening and thus reduces disturbed flow patterns at the proximal and distal edges.

Although, critical to understanding healing and long term performance of stents, these dynamic WSS alterations are difficult to measure in vivo as it would require detailed invasive measurements at different time points.

The utilization of computational modeling techniques to assess the performance of isolated or virtually deployed coronary stents has been proven to be an important tool to predict their mechanical behavior over time. These numerical simulations provide a preliminary “proof-of-concept” for new technologies to further qualify from bench to clinical application.[5]

Herein, we provide a series of three-dimensional simulations in idealized geometries focusing at the strut level in two different time points: 1. stage I, which represents the post-implantation stage of the virtually deployed scaffold and 2. stage II, which represents the time point where 33% of scaffold resorption has been achieved. Each of these stages focus on the anatomic configuration of the struts. In particular 3 distinct surfaces were defined: 1. Lateral inflow surface (a) where the strut surface faces the inflow area, 2. Lateral outflow surface (c) where the strut surface faces the outflow area and 3. Endoluminal surface or top of the strut (b) facing towards the lumen. During stage II, two distinct phenomena take place: 1. Neointimal tissue generation and 2. Bulk resorption of the scaffold, which affects its spatial dimensions, and subsequently local flow conditions (Electronic Supplement).

Our goal was to test the hypothesis that local hemodynamic conditions derived from advanced CFD simulations change, as the virtually applied bioresorption progresses over time. These observations may potentially translate to improved flow patterns over the scaffolded segments or the scaffold edges which in the clinical setting affect local tissue responses (Figures 1–3).

METHODOLOGY

Computational fluid dynamics

Blood was approximated to behave as a Newtonian fluid with a density of 1 g/cm^3 and constant viscosity of 0.04 g/cm/sec for CFD simulations. Flow velocity and pressure in the coronary artery were computed by numerically solving the unsteady Navier-Stokes equations, which represent conservation of mass and balance of momentum. The spatial discretization of the Navier-Stokes equations was based on the Galerkin FEM. In particular, a piecewise linear approximation was adopted for pressure and piecewise quadratic for velocity. Time discretization was achieved with a semi-implicit backward Euler method with a time step of $5 \times e^{-4}$ s. CFD simulations and post processing were carried out

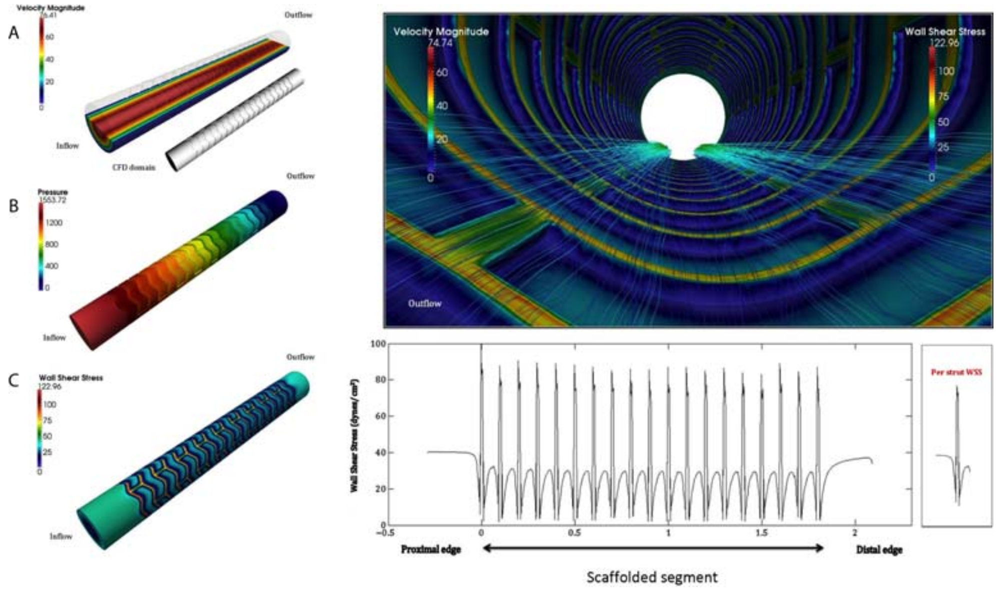

Figure 1. Numerical modeling of the virtually deployed bioresorbable scaffold in an idealized straight geometry (post-procedure or stage I). CFD simulations visualizing the velocity streamlines and WSS magnitude on the endoluminal and lateral outflow surfaces of the struts following virtual scaffold deployment. Plot of the quantified WSS vs. axial distance on the endoluminal and both strut sides at stage I. Panels A, B, C: Velocity magnitude, pressure and wall shear stress distribution over the CFD domain.

based on LifeV (EPFL, Switcherland; Politecnico di Milano, Italy; INRIA, France; and Emory University, USA), for numerical solution of partial differential equations. The CFD model consisted of the: 1. geometric construction of the scaffolded vessel; 2. meshing of geometry; 3. imposition of proper boundary conditions and quantities of interest. In brief the boundary conditions are applied at the inlet (proximal) and outlet (distal) surfaces of the CFD domain (the region where the blood is flowing) (Figure 1: Panels A, B, C & Figure 2: Panels A, B, C).

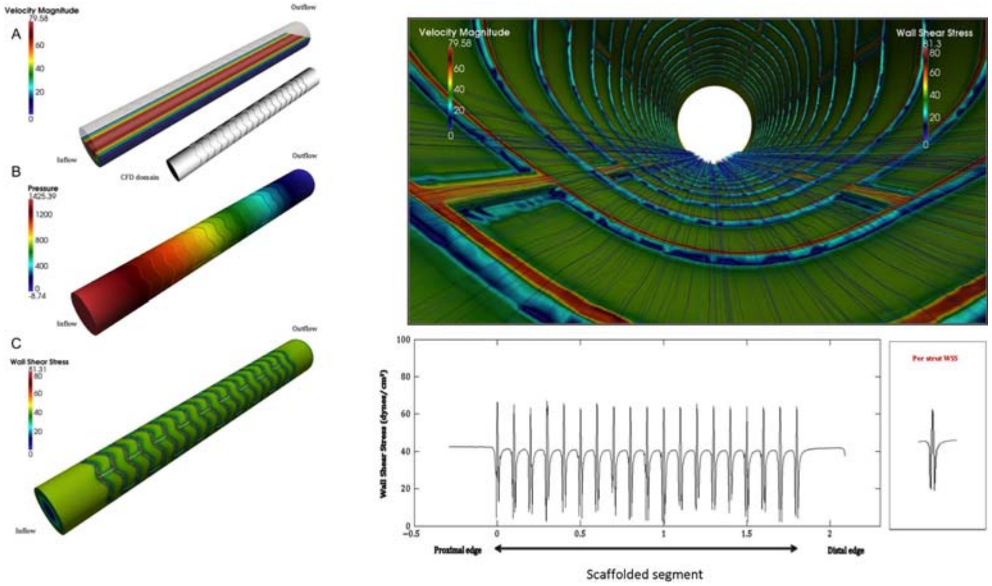

Figure 2. Numerical modeling of the virtually applied bioresorption in an idealized straight geometry (follow-up or stage II). CFD simulations visualizing the velocity streamlines and WSS magnitude on the endoluminal and lateral outflow surfaces of the struts following virtually applied bioresorption. Plot of the quantified WSS vs. axial distance on the endoluminal and both strut sides at stage II. Panels A, B, C: Velocity magnitude, pressure and wall shear stress distribution over the CFD domain.

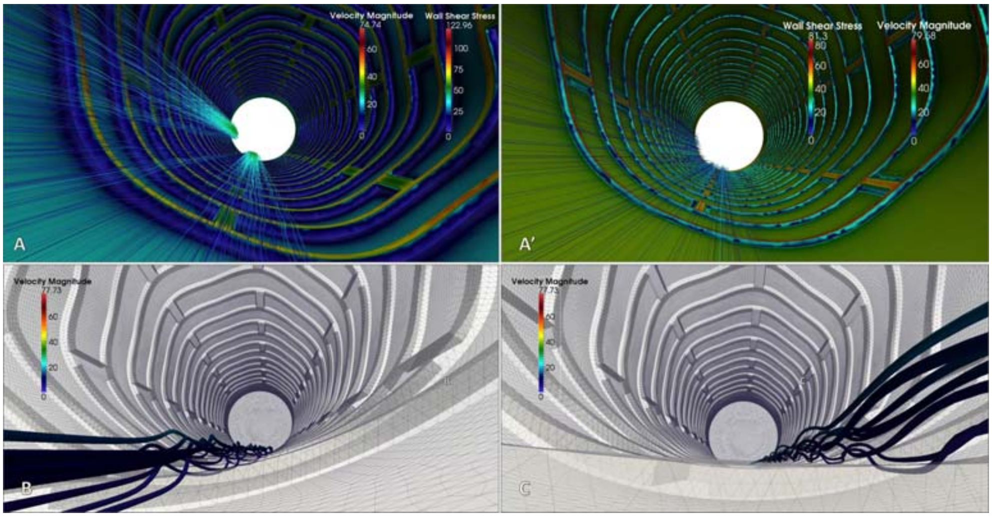

Figure 3. Numerical modeling of the simulated stage I (post-procedure) and stage II (virtually applied bioresorption) at the distal edge in an idealized straight geometry. Panels A& A′: CFD simulations of the velocity profiles, pressure and WSS at strut # 19 (distal edge) Panels B, B′: CFD simulations of the velocity magnitudes visualizing the altered flow patterns over the virtually deployed struts.

Geometric reconstruction of the scaffolded vessel

The geometry of the deployed scaffold was constructed based on the structure of an actual 3.0 × 18 mm Absorb BVS (Abbott Vascular, SC, Calif.) utilizing the validated software Rhino 5.0 (www.rhino3D.com) for solid modeling. We modeled 19 horizontal rings interconnected by 3 vertical bridges. We performed simulations in two idealized vessel geometries, a straight vessel and a curved vessel with a 90° angle. We examined 2 stages in each vessel model Stage I: post-implantation, where the strut thickness is 0.015 cm (150 μm); the distance between each strut 0.1 cm, the degree of embedding in the vessel wall 50% simulating half-embedded struts, (the distance between the endoluminal and abluminal strut surface: 0.0075 cm) and the radius of the vessel lumen 0.15 cm and stage II: follow-up, where the strut thickness is reduced to 0.010 cm (67%) reflecting a 33% strut bioresorption and the radius of the lumen reduced to 0.14975 cm simulating some degree of bioresorption and neointimal hyperplasia (NIH), respectively.

Since we are interested in the changes in WSS around the struts we defined three different strut surfaces: 1. Lateral inflow, the surface facing the inflow area, 2. Lateral outflow, the surface facing the outflow area and 3. Endoluminal strut surface, the top surface of the strut (Electronic Supplement).

Meshing of geometry

The geometry volume was discretized as an unstructured mesh of tetrahedral elements using Netgen (Linz, Australia) and Gmsh (http://geuz.org/gmsh/). Since the region of interest is close to the boundaries (wall and struts), we computed a mesh featuring more refined elements (resulting in a more accurate numerical solution) in these regions. In view of the complexity of the geometry induced by the stent the meshing process is split in two steps where the boundary layer with thickness 0.025 cm and mesh size of 0.004 cm are computed with NetGen and the lumen is filled by GMsh. Both packages offer implementation of cutting-edge mesh optimization algorithms.

Imposition of boundary conditions and quantities of interest

We prescribed a steady and maximum inflow rate of 2.7 cm^3/sec, under normal conditions. The vessel wall was assumed as rigid for the sake of computational time; however extension to the deformable case is feasible as well. The quantities of interest were the velocity (cm/sec), pressure (dynes) and wall shear stress (dynes/cm^2) in the CFD domain. Flow rate was prescribed by means of a parabolic velocity profile properly adjusted to the desired boundary condition.

Statistical analysis

Variables are presented as average values. Change (difference) for each variable was estimated as: follow-up minus post-procedure (or stage II-stage I). Percent change was calculated as:

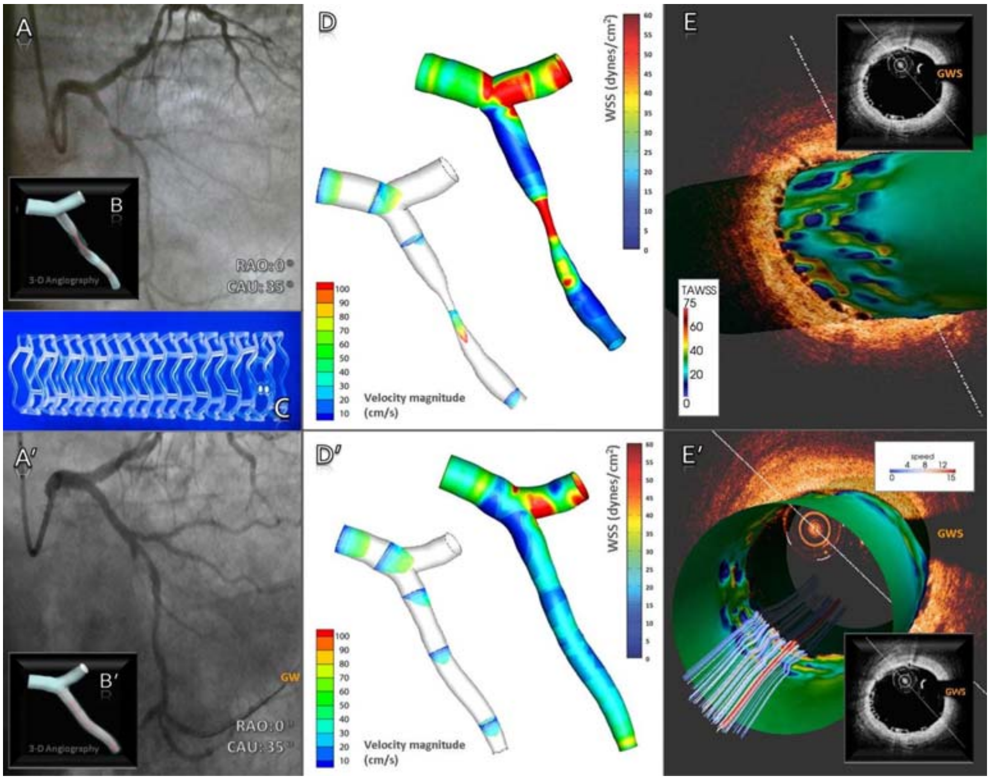

Figure 4. Computational Fluid Dynamic Simulations derived from optical coherence tomographic imaging (reproduced by permission[11]). (A, A′) Two-dimensional (2-D) angiographic views of the significant proximal left circumflex artery lesion (A) and the scaffolded segment after implantation of a 3.0 18-mm Absorb bioresorbable vascular scaffold (BVS). (B, B′) Three-dimensional (3-D) angiographic views before (B) and after (B′) scaffold implantation. (C) The Absorb BVS. (D, D′) Time-averaged wall shear stress (TAWSS) magnitude distribution from angiographically derived 3-D geometries before (D) and after (D′) scaffold deployment. Velocity profiles pre- and post-implantation of the Absorb BVS are superimposed. (E) 2-D OCT cross section with embedded polymeric struts demonstrating in a 3-D pattern the distribution of TAWSS between the polymeric struts. The quantified color coding demonstrates low WSS regions (blue color). The matched OCT cross section is superimposed. (E′) Reconstructed streamlines of the velocity field at the systolic peak demonstrating altered flow patterns in the proximity of the arterial wall induced by the polymeric struts. CFD = computational fluid dynamics; GWS = guidewire shadow.

follow-up-post-procedure/ post-procedure x 100% (or stage II- stage I/ stage I x 100%). Data analysis was performed with SPSS 19 for Mac (SPPSS, Chicago, IL).

RESULTS

In-scaffold, straight vessel

The average WSS values following virtual scaffold deployment (stage I) over the inflow and outflow strut surfaces were 3.2 and 3.1 dynes/cm^2, respectively and 87.5 dynes/cm^2 at the endoluminal strut surface. The percent (%) WSS increased from stage I to stage II by 100% and 142% over the inflow and outflow surfaces respectively, and decreased by 27% over the endoluminal surface (Figure 5A).

In-scaffold, curved vessel

The average WSS of the inner curvature at stage I over the inflow and outflow strut surfaces were 4.3 and 2.9 dynes/cm^2, respectively, and at the endoluminal strut surface was 88.6 dynes/cm^2. Similar analysis of the outer curvature demonstrated WSS values of similar magnitude: 5.8, 3.9 and 118.1 dynes/cm^2 respectively. The WSS from stage I to stage II at the inner curvature increased by 63% in the inflow and by 66% in the outflow surface and decreased by 20% over the endoluminal surface. Similarly, at outer curvature the %WSS increased at the inflow and outflow surfaces by 29% and 56%, respectively, and decreased over the endoluminal surface by 28% (Figure 5B).

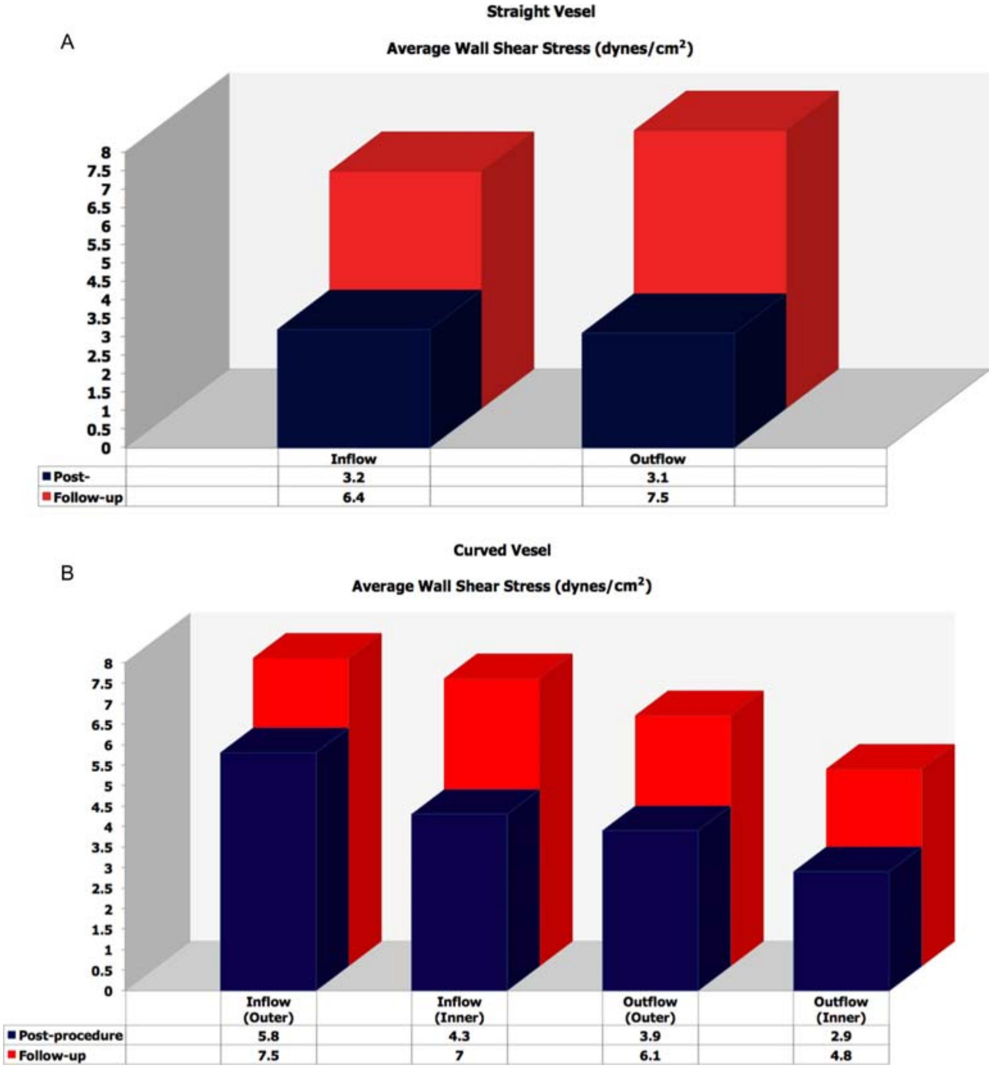

Figure 5. WSS quantification over the simulated strut surfaces at stages I and II in (A) straight and (B) curved idealized geometries.

Edge, straight vessel

The average WSS following virtual scaffold implantation over the inflow surface of the proximal edge did not change significantly, however over the outflow surface of the proximal edge changed significantly: from 2.2 to 12.9 dynes/cm^2, a percentile increase of 486%. At the distal edge percentile WSS increased by 59% at the inflow and by 79% over the outflow surface (Figure 6).

Edge, curved vessel

In curved vessels, the average WSS change of the inflow and outflow strut surfaces of the proximal edge at the inner curvature increased by 79% and 66% respectively. At the distal edge similar analysis showed decrease by 67% and 3% respectively (Table 1).

DISCUSSION

Computational fluid dynamics simulations performed in this study demonstrate that: 1) immediately post scaffold deployment WSS is high at the endoluminal strut surface and very low at the lateral inflow and lateral outflow regions of each strut; 2) at a time point when 33% of scaffold bioresorption occurs, the WSS reduces by approximately 30% at the endoluminal strut surface and increases by over 100% at the inflow and outflow regions of each strut resulting in a more uniform distribution of WSS across the endoluminal and lateral strut surfaces; 3) these findings were more pronounced at the inner

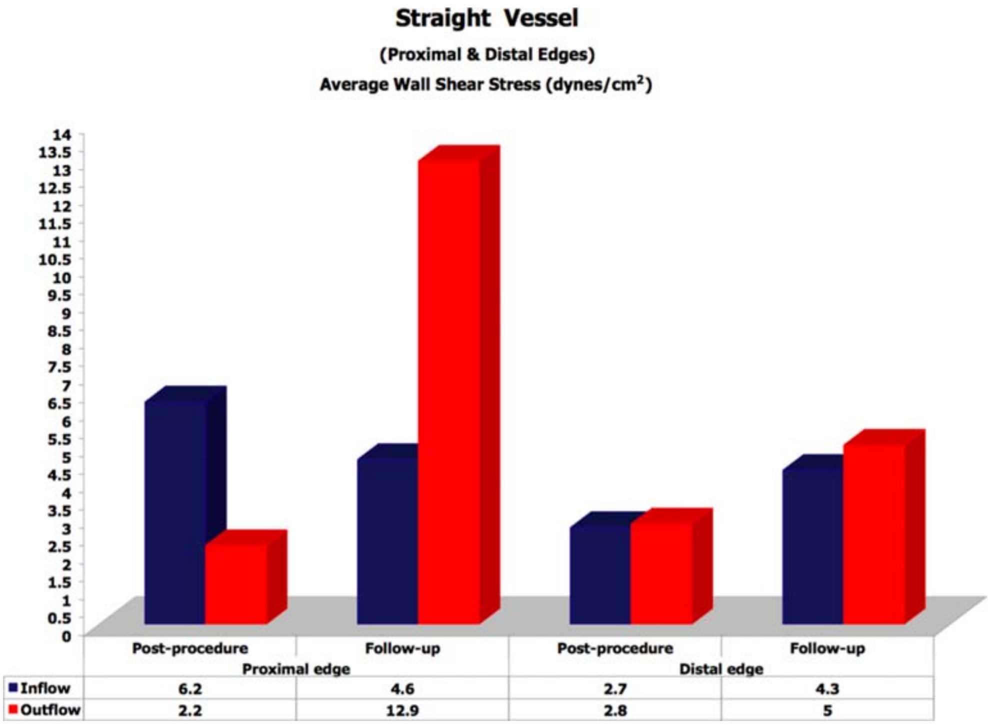

Figure 6. WSS quantification over the simulated strut surfaces of the proximal and distal edges at stages I and II in straight idealized geometries.

curvature than the outer curvature of curved vessels; and 4) WSS is very low at the scaffold edges immediately after scaffold deployment, variably changes at follow up but remains low enough to incite an edge neo-intimal response.

Dynamic endoluminal WSS and neointimal formation with bioresorbable scaffolds

It is known that low WSS such as created at the lateral inflow and outflow strut surfaces, promotes activation, migration, and phenotype shift of smooth muscle cells from a contractile to a more synthetic phenotype with production of extracellular matrix through up-regulation of the smooth muscle cell differentiation repressors: platelet-derived growth factor and KLF-4.[4,6] These biologic responses initiate a neointima that fills in between the struts of the scaffold thereby reducing the effective thickness of the struts and increasing the value of WSS at the strut inflow and outflow. Simultaneously, bulk resorption of the strut results in a smaller and thinner effective strut thereby lowering the magnitude of the high WSS at the endoluminal strut surface. The net effect of this sequence of events is that the large variability of WSS around bioresosrbable struts immediately after deployment (stage I) smoothens out when 33% of the struts are resorbed (stage II). Although no absolute WSS cutoff value after stent deployment has been definitively shown to predict an intense neointimal response, WSS values <0.5 Pa (5 dynes/cm^2) maybe a ongoing stimulus for neointimal hyperplasia precipitating in-segment restenosis.[7–9]

Table 1. WSS quantification over the simulated proximal and distal edges in stages I and II in a curved geometry.

Curved Vessel Average WSS (dynes/cm^2)	Post-	Follow-Up	Relative Change (%)	Post-	Follow-Up	Relative Change (%)
	Inner Curvature: Proximal edge			*Inner Curvature: Distal edge*		
Inflow	7.7	13.8	79	9.0	3.0	−67
Endoluminal surface	126.1	87	−31	68.5	58	−15
Outflow	5.6	9.3	66	7.9	7.7	−3
	Outer Curvature: Proximal edge			*Outer Curvature: Distal edge*		
Inflow	6.8	5.2	−24	9.3	3.4	−63
Endoluminal surface	85.8	53.5	−38	170	117.8	−31
Outflow	2.0	3.9	95	2.4	4.9	104

In our models simulating a bioresorbable scaffold with strut thickness of 150μm and rectangular strut geometry, WSS was frequently noted to be <0.5 Pa in the lateral strut surfaces and always significantly ≥ 0.5 Pa at the endoluminal strut surface immediately after scaffold deployment. We found that following 33% bioresorption, WSS in lateral strut surfaces significantly increased and WSS at the endoluminal strut surface significantly decreased. These observations may reflect a biphasic tissue response with accelerated tissue proliferation in the low WSS segments in the lateral strut surfaces early post-implantation that subsequently plateaus when WSS rises above the threshold that promotes hyperplasia. Although we didn't model more advanced time points in the resorption process, the peak and trough values of WSS in the endoluminal strut surface and the lateral strut surfaces with ongoing scaffold resorption continue to approximate one another until such time as the scaffold is fully degraded and the ongoing low WSS stimulus for neointimal hyperplasia between the struts is extinguished. This smooth surface and laminar hemodynamic environment is likely atheroprotective and conducive to a clinically stable vessel with appropriate medical therapy and risk factor modification. One can speculate that such a smooth surface created by a well healed bioresorbable scaffold can be applied towards plaque sealing and shielding. Clinical data supporting this notion are provided from a recent study of 58 patients who underwent Absorb BVS implantation for stable ischemic heart disease and acute coronary syndromes with optical coherence tomography imaging at 12 months demonstrating a robust neointimal layer that provides a thick fibrous cap overlying residual plaques.[10]

The feasibility of 3-D WSS reconstructions derived from two-dimensional OCT acquisitions following implantation of bioresorbable scaffolds has been recently described[11] (Figure 4). The further association of local 3-D WSS alterations with underlying neointimal proliferation utilizing advanced light-based imaging remains to be elucidated in real-world randomized human data.

Clearly scaffold design, strut thickness, strut shape (rectangular, circular, elliptical or tear-drop shape) and the scaffold resorption rate will significantly impact the near wall-flow patterns (micro-environment), vascular hemodynamic milieu (macro-environment) and resulting time frame of vascular response. In contrast to this complex dynamic environment with transient scaffolds, the design of metallic stents has a sustained impact over the regional hemodynamic micro- and macro-environments. Indeed, rigid metallic stents have been shown to increase vascular angulation in the proximal stent edge by 121% and the distal edge by 100%, inducing regions of low WSS at these edges which were associated with a robust neo-intimal response.[12–13] We have hypothesized that more compliant metallic stents and to a greater extent bioresorbable scaffolds deployed in curved and angulated vessels will have less straightening effect at device edges and in the case of bioresorbable scaffolds will restore vessel geometry after the completion of bioresorption process.[14–15]

Edge WSS and neointimal formation

Edge restenosis accounts for approximately 6% of target lesion revascularization rates and manifests with both metallic and bioresorbable devices.[16–17] The magnitude of proximal and distal edge vascular responses has been previously shown to be associated with the stent or scaffold design and strut thickness, axial and longitudinal geographical miss,[18] underlying tissue composition at the landing zone,[19] and variable straightening of the stented segment at the edges.[12,20] The magnitude of altered flow patterns which influence local WSS distributions and subsequently influence tissue proliferation have been numerically demonstrated in our model providing additional evidence for the association of flow-mediated tissue responses at the transition zones.

CONCLUSIONS

The present study applied computational fluid dynamics to simulate the biologic behavior of virtually deployed bioresorbable scaffolds. This is the first proof-of-concept which potentially applies clinical translations for further development of bioresorbable platforms.

LIMITATIONS

There are several limitations in this analysis which have to be addressed. Firstly the idealized geometry and the rigidity of the vessel wall are considered as major limitations of the current study as well as the resorption process which was assumed to be uniform. Cardiac torsion may induce local stresses over the scaffolded segments and increase the rate of absorption at the struts exposed in higher local forces. Secondly the virtually modeled neointimal tissue was assumed to have a symmetric distribution over the scaffolded segment and prior studies with advanced light-based imaging such as optical coherence tomography have shown that eccentric pattern of neointimal generation is also possible. Thirdly the flow conditions in this model were assumed to be steady and the boundary conditions were not patient specific.

REFERENCES

[1] Grube E, Schofer J, Hauptmann KE, Nickenig G, Curzen N, Allocco DJ, Dawkins KD. A novel paclitaxel-eluting stent with an ultrathin abluminal biodegradable polymer 9-month outcomes with the JACTAX HD stent. *JACC Cardiovasc Interv.* 2010 Apr;3(4):431–438.
[2] Park SJ, Kang SJ, Virmani R, Nakano M, Ueda Y. In-stent neoatherosclerosis: A final common pathway of late stent failure. *J Am Coll Cardiol.* 2012 Jun 5;59(23):2051–2057.
[3] Wykrzykowska JJ, Onuma Y, Serruys PW. Vascular restoration therapy: The fourth revolution in interventional cardiology and the ultimate “rosy” prophecy. *EuroIntervention.* 2009 Dec 15;5(Suppl F):F7–F8.
[4] Koskinas KC, Chatzizisis YS, Antoniadis AP, Giannoglou GD. Role of endothelial shear stress in stent restenosis and thrombosis: Pathophysiologic mechanisms and implications for clinical translation. *J Am Coll Cardiol.* 2012 Apr 10; 59(15):1337–1349.
[5] Formaggia L, Quarteroni A, Veneziani A. *Cardiovascular Mathematics*. Milan: Springer; 2009.
[6] Chatzizisis YS, Coskun AU, Jonas M, Edelman ER, Feldman CL, Stone PH. Role of endothelial shear stress in the natural history of coronary atherosclerosis and vascular remodeling: Molecular, cellular, and vascular behavior. *J Am Coll Cardiol.* 2007 Jun 26;49(25):2379–2393.
[7] Liu SQ, Goldman J. Role of blood shear stress in the regulation of vascular smooth muscle cell migration. *IEEE Trans Biomed Eng.* 2001 Apr;48(4):474–483.
[8] Nerem RM. Hemodynamics and the vascular endothelium. *J Biomech Eng.* 1993 Nov;115(4B):510–514.
[9] Van der Heiden K, Gijsen FJ, Narracott A, Hsiao S, Halliday I, Gunn J, Wentzel JJ, Evans PC. The effects of stenting on shear stress: Relevance to endothelial injury and repair. *Cardiovasc Res.* 2013 Jul 15;99(2):269–275.
[10] Brugaletta S, Radu MD, Garcia-Garcia HM, Heo JH, Farooq V, Girasis C, van Geuns RJ, Thuesen L, McClean D, Chevalier B, Windecker S, Koolen J, Rapoza R, Miquel-Hebert K, Ormiston J, Serruys PW. Circumferential evaluation of the neointima by optical coherence tomography after ABSORB bioresorbable vascular scaffold implantation: Can the scaffold cap the plaque? *Atherosclerosis.* 2012 Mar;221(1):106–112.
[11] Gogas BD, King SB 3rd, Timmins LH, Passerini T, Piccinelli M, Veneziani A, Kim S, Molony DS, Giddens DP, Serruys PW, Samady H. Biomechanical assessment of fully bioresorbable devices. *JACC Cardiovasc Interv.* 2013 Jul;6(7):760–761.
[12] Wentzel JJ, Whelan DM, van der Giessen WJ, van Beusekom HM, Andhyiswara I, Serruys PW, Slager CJ, Krams R. Coronary stent implantation changes 3-D vessel geometry and 3-D shear stress distribution. *J Biomech.* 2000 Oct;33(10):1287–1295.
[13] Thury A, Wentzel JJ, Vinke RV, Gijsen FJ, Schuurbiers JC, Krams R, de Feyter PJ, Serruys PW, Slager CJ. Images in cardiovascular medicine. Focal in-stent restenosis near step-up: Roles of low and oscillating shear stress? *Circulation.* 2002 Jun 11;105(23):e185–e187.
[14] Gomez-Lara J, Garcia-Garcia HM, Onuma Y, Garg S, Regar E, De Bruyne B, Windecker S, McClean D, Thuesen L, Dudek D, Koolen J, Whitbourn R, Smits PC, Chevalier B, Dorange C, Veldhof S, Morel MA, de Vries T, Ormiston JA, Serruys PW. A comparison of the conformability of everolimus-eluting bioresorbable vascular scaffolds to metal platform coronary stents. *JACC Cardiovasc Interv.* 2010 Nov;3(11):1190–1198.
[15] Serruys PW, Garcia-Garcia HM, Onuma Y. From metallic cages to transient bioresorbable scaffolds: Change in paradigm of coronary revascularization in the upcoming decade? *Eur Heart J.* 2012 Jan;33(1):16–25b.
[16] Gogas BD, Garcia-Garcia HM, Onuma Y, Muramatsu T, Farooq V, Bourantas CV, Serruys PW. Edge vascular response after percutaneous coronary intervention: An intracoronary ultrasound and optical coherence tomography appraisal: From radioactive platforms to first- and second-generation drug-eluting stents and bioresorbable scaffolds. *JACC Cardiovasc Interv.* 2013 Mar;6(3):211–221.
[17] Gogas BD, Bourantas CV, Garcia-Garcia HM, Onuma Y, Muramatsu T, Farooq V, Diletti R, van Geuns RJ, De Bruyne B, Chevalier B, Thuesen L, Smits PC, Dudek D, Koolen J, Windecker S, Whitbourn R, McClean D, Dorange C, Miquel-Hebert K, Veldhof S, Rapoza R, Ormiston JA, Serruys PW. The edge vascular response following implantation of the Absorb everolimus-eluting bioresorbable vascular scaffold and the XIENCE V metallic everolimus-eluting stent. First serial follow-up assessment at six months and two years: Insights from the first-in-man ABSORB Cohort B and SPIRIT II trials. *EuroIntervention.* 2013 Oct 22;9(6):709–720.
[18] Costa MA, Angiolillo DJ, Tannenbaum M, Driesman M, Chu A, Patterson J, Kuehl W, Battaglia J, Dabbons S, Shamoon F, Flieshman B, Niederman A, Bass TA, STLLR Investigators. Impact of stent deployment procedural factors on long-term effectiveness and safety of sirolimus-eluting stents (final results of the multicenter prospective STLLR trial). *Am J Cardiol.* 2008 Jun 15;101(12):1704–1711.
[19] Waxman S, Freilich MI, Suter MJ, Shishkov M, Bilazarian S, Virmani R, Bouma BE, Tearney GJ. A case of lipid core plaque progression and rupture at the edge of a coronary stent: Elucidating the mechanisms of drug-eluting stent failure. *Circ Cardiovasc Interv.* 2010 Apr;3(2):193–196.
[20] McDaniel MC, Samady H. The sheer stress of straightening the curves: Biomechanics of bioabsorbable stents. *JACC Cardiovasc Interv.* 2011 Jul;4(7):800–802.